STRUCTURAL HEALTH MONITORING OF COMPOSITE STRUCTURES

by

Pooja Mehta

A thesis submitted to the faculty of
The University of Utah
in partial fulfillment of the requirements for the degree of

Master of Science

Department of Electrical and Computer Engineering

The University of Utah

August 2017

The University of Utah Graduate School

STATEMENT OF THESIS APPROVAL

The thesis of **Pooja Mehta**
has been approved by the following supervisory committee members:

Joel B. Harley ,	Chair(s)	**18 April 2017** Date Approved
Rong-Rong Chen ,	Member	**18 April 2017** Date Approved
Tolga Tasdizen ,	Member	**18 April 2017** Date Approved

by **Gianluca Lazzi** , Chair/Dean of
the Department/College/School of **Electrical and Computer Engineering**
and by **David B. Kieda** , Dean of The Graduate School.

ABSTRACT

Carbon fiber-reinforced composite materials have been increasingly used in aerospace and aeronautics industries due to their superior strength over metals, low fatigue life, high corrosion resistance, and temperature resistance. Since most damage, such as delaminations, manifest inside the composite material, we often cannot detect damage through visual inspection. As a replacement for visual inspection, ultrasonic guided waves have been widely researched to remotely detect, locate, and characterize damage in structures due to their unique capability to travel long distances and inspect inaccessible locations for damage. Yet the anisotropic nature of composites makes it difficult to identify the velocity characteristics of the guided waves and utilize them for damage localization.

To address this challenge, we use sparse wavenumber analysis to determine anisotropic multimodal and dispersive frequency-wavenumber characteristics of guided waves. We then use these multimodal and dispersive properties to predict how guided waves propagate in the anisotropic plate through sparse wavenumber synthesis. Finally, these predictions, which form a wave propagation model for the composite, are integrated with matched field processing, a model-based localization framework, to locate damage on the composite.

For my family, Rachna, Arun, Anisha, Pushkar, and Amol

CONTENTS

LIST OF FIGURES

ACKNOWLEDGEMENTS

I would like to thank Dr. Joel B. Harley for giving me an opportunity to do research under him. I am extremely grateful for his help keeping me on track with patient criticism and guidance. He provided the praise, support, and constructive criticism that every student needs to flourish. The door to his office was always open whenever I ran into trouble or had a question about my research or writing. I am also grateful for his thesis writing sessions.

I would like to thank my committee members Dr. Rong-Rong Chen and Dr. Tolga Tasdizen for imparting valuable skills and for their interest in my work.

I thank all the students of Wave Integrated Signal Processing (WISP) group that supported me and for their valuable suggestions. I am fortunate to have an excellent work environment in the laboratory which facilitated my work to a great deal.

Finally, I am grateful for the tremendous support and motivation of my family for providing me with unfailing support and continuous encouragement throughout my years of study and through the process of researching and writing this thesis. This accomplishment would not have been possible without them. Thank you.

CHAPTER 1

INTRODUCTION

1.1 Motivation

Structural health monitoring is the process of detecting, locating, and characterizing damage in structures, such as bridges [1], aircrafts [2], and gas pipelines [3]. Damage to these structures can occur due to earthquakes, fires, or other catastrophic events that may lead to loss of life and property. Monitoring the health of structures is desired to reduce maintenance costs through predictive maintenance rather than periodic maintenance [4]. Predictive maintenance avoids removing the parts where there is no defect and hence reduces the maintenance cost. Structural health monitoring is done by collecting and monitoring data of a structure over an extended period of time using sensors and then analyzing the data to identify the health of the structure.

Monitoring aging structures is crucial for detecting and stopping potential problems before they grow into catastrophic failures. On June 1983, Mianus River Bridge in United States collapsed due to metal corrosion and deferred maintenance [5]. Aging of the bridge was also one of the reason for its collapse. Therefore, to ensure the safety of people, it is important to improve the maintenance of structures, which has become possible due introduction of structural health monitoring [4].

The process of structural health monitoring consists of mounting sensors on a structure and collecting and monitoring the data to analyze the health of the structure. Structural health monitoring also reduces human labor as these sensors monitor the status of the structure continuously without human intervention. This minimizes the probability of human error, which might include faults going undetected, and hence improves the reliability of structures.

Over the last few decades, SHM has been primarily developed to detect damage on metal structures [6]. Metal structures, such as machine parts of wind turbines, satellites, and other components are often used beyond their lifetimes [6] and proper maintenance

and monitoring is required for their further use. Many SHM challenges have been already solved for metal structures and now focus is on solving the SHM challenges for composite structures.

In the last decade, composite materials have been increasingly used in the aerospace and aeronautics industries [7] due to their superior strength over metals [8], low fatigue life [9], high corrosion resistance [10], and temperature resistance [10]. Composites are anisotropic in nature. That is, the waves in composites travel with different propagating speeds in different directions. Unlike in metals, there are not many well-defined wave propagation models for composites. Therefore, it is difficult to accurately identify how waves propagate in a composite material. Also, unlike metals, we can often not visually see damage (e.g., dents) in a composite plate [11]. This leads to difficulty in detecting damage in composites. Hence, detecting damage in composite structures is exceedingly important. Damage refers to any undesirable change in the geometric or material properties of the structure. For composites, defects refer to fiber waviness [12], delamination (repeated impact/ stress causes the layers to separate) [13], porosity [14], etc. These defects can occur during manufacturing or in-service operations. As a result, non-destructive evaluation (NDE) techniques are necessary to accurately detect and locate damage.

There are many non-destructive evaluation modalities. One of the most common is ultrasonic testing [15]. Among the ultrasonic testing methods, this proposal focuses on ultrasonic guided waves. Ultrasonic guided waves are waves that are guided by the structure of the material in which they propagate. These waves are used due to their sensitivity to material variations, ability to travel long distances in a structure, and unique capability to travel to inaccessible locations for damage detection. Hence, guided waves are used to remotely detect, locate, and characterize damage in physical structures [16].

Ultrasonic guided waves are waves that are guided by the structure of the material in which they propagate. Guided waves have been successfully used to detect and locate damage in many isotropic metals [16]. More recent work has applied guided waves to composites as well [17]. Yet, due to the anisotropic nature of many composites, traditional isotropic signal processing methods fail [18, 19]. This is, in part, generally due to not knowing the velocity characteristics of guided waves. In this thesis, we will use sparse wavenumber analysis [15] to determine the frequency-wavenumber (or phase velocity)

characteristics of the guided waves from small sets of measurements. This approach uses algorithms from compressive sensing to recover multimodal and dispersive properties (wavenumbers and complex amplitudes) of guided waves.

We will use these multidimensional multimodal and dispersive properties (known as dispersion curves) to predict how guided waves propagate in the entire anisotropic plate. This process is known as sparse wavenumber synthesis [15]. Finally, these predictions (i.e., a wave propagation model for the composites) are integrated with matched field processing [20], a model-based localization framework, to locate a transmitter source (e.g., a sensor) or a damage. In prior work, sparse wavenumber analysis, sparse wavenumber synthesis, and matched field processing were used to locate damage in isotropic plates [17]. We further expand and improve this framework to locate damage in an anisotropic plate by predicting guided wave behavior at any location in the structure.

1.2 Background

1.2.1 Composites

A composite material is made from combination of different materials with different physical or chemical properties, which produces a material with characteristics that are far different from each individual material. A composite material has the advantage of combining a number of properties that are generally not found together in a single material. A combination of polymer matrix and fiber reinforcement materials is referred to as fiber reinforced plastic. Carbon fiber reinforced composites are made of layers (i.e., lamina) of carbon fiber sheets. Each sheet has its own particular mechanical properties. If all the fibers of a single layer are aligned in a single direction, the material will be stiff parallel to the fibers, but flexible perpendicular to the fibers. After many of these layers are orientated, stacked together, and joined with a resin epoxy matrix, we can design a new material with different mechanical properties.

Composites are light in weight, have high strength (usually in a particular direction), are corrosion resistant, and can be molded into complicated shapes compared to metals. Composite materials are used for many structures, including buildings, bridges, and structures such as bathtubs and storage tanks [21]. Fiber-reinforced composite materials typically exhibit anisotropy. That is, some properties of the composite vary depending

upon which geometric plane they are measured along. This leads to difficulty in predicting the velocity characteristics of waves traveling in a composite.

Most defects in composites occur under the surface of the composite and are undetectable by visual inspection. Common defects in composites include delamination, fiber waviness, and porosity. These defects are described in the following subsections.

1.2.1.1 Delamination

Delamination is produced due to repeated impact or stress that causes the layers of the composite to separate. Delamination happens within the composite structure and is not visible on the surface. This leads to reflections in the delaminated region and does not allow the wave energy to leave the delaminated region, causing the waves to be attenuated traveling in that region [22]. Our method can detect and localize delaminations.

1.2.1.2 Fiber Waviness

Fiber waviness refers to improper orientation of fibers [23]. It occurs during the manufacturing of composites. It can be classified into in-plane and out-of-plane fiber waviness. In in-plane fiber waviness, fibers are misaligned in the direction of the fiber plane [24]. As a result, guided waves will propagate less efficiently in directions of the fibers and more efficiently in directions perpendicular to the fibers. In case of out-of-fiber waviness, fibers are misaligned in directions perpendicular to the direction of the fiber. But this affects the guided waves in all directions [23]. Fiber waviness leads to a change in anisotropy of the composite and our model does not incorporate the parameters to detect them.

1.2.1.3 Porosity

Porosity refers to small pores or voids in the matrix of the composite. Voids can include air bubbles or solvents like chemicals used to clean the surface [100]. Porosity can be caused due to incorrect parameters like temperature or pressure of resin and can significantly affect the strength of composites [25]. Porosity leads to a change in velocity characteristics of the waves [26]. Our model does not incorporate the parameters to detect porosity.

These defects occur during manufacturing or in-service operations and are not visible on the surface. As a result, non-destructive evaluation (NDE) and SHM techniques are

necessary to accurately detect and locate these types of damage.

1.2.2 Ultrasonic Guided Waves

Guided waves are low-frequency stress waves that propagate in a structure, guided by its boundaries. Guided waves are used in different fields. Rayleigh and Love waves are guided waves used in geodynamics and seismology [27]. Rayleigh waves are generated during earthquakes and are used to characterize the interior of the earth, such as to locate oil deposits [28]. They travel along the surface of solids [29]. Love waves are surface waves having horizontal motion that is perpendicular to the direction of wave propagation [30].

Guided waves in a plate are called Lamb waves [31]. Lamb waves are guided by the plate in which they propagate and form interference patterns across the plate's thickness. These waves are commonly used in structural health monitoring due to their ability to travel over long distances with low attenuation. Ultrasonic guided waves allow inspection of large, complex structures using limited numbers of sensors. An illustration of a guided wave measurements in a composite is shown in Figure 1.1(a). Lamb waves are characterized by multimodal (creating multiple wave excitations) and dispersive (distinct frequency-dependent velocities) wave propagation [16]. These wave modes are typically divided into two families: symmetric and antisymmetric modes, as shown in 1.1(b). Symmetric wave modes vibrate in the direction of plate length, whereas the antisymmetric wave modes vibrate in direction perpendicular to the plate length. As frequency increases

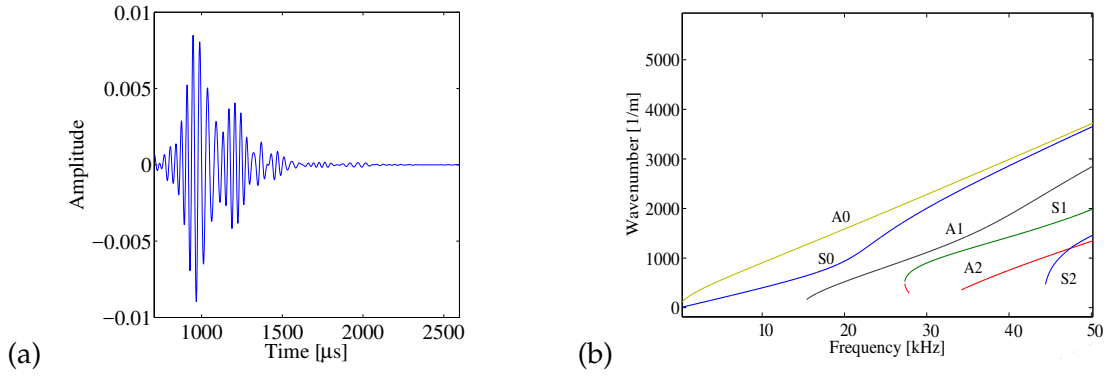

Figure 1.1. Illustration of (a) Guided wave between a pair of sensors in a composite plate. (b) Dispersion curves obtained from solving the Rayleigh-Lamb equation. Asymmetric wave modes are denoted by A0, A1 and A2. Symmetric wave modes are denoted by S0, S1 and S2.

(in Figure 1.1(b)), more wave modes are created at different cut-off frequencies, with each wave mode traveling with different velocities. Often these velocities are also affected by environmental factors like temperature. These environmental factors contribute to the complexity of accurately characterizing guided waves.

1.2.2.1 Guided Wave Localization in Isotropic Structures

Traditional delay-and-sum algorithms are often used to locate damage in isotropic plates [18]. Fromme [32] applied delay-and-sum to locate defects in a steel plate. Michaels [33] used the delay-and-sum algorithm to locate notch and corrosion on an aluminum plate. In delay-and-sum, the received signal is modeled as the delayed replica of the original transmitted signal $x(t)$.

Specifically, delay-and-sum localization models the signal at the receiver i as [33–35]

$$y_i(t) = x\left(t - \frac{D}{V}\right) \tag{1.1}$$

where D is the distance between transducer pairs and V is the group velocity of the dominant wave mode. The residual signals from various transmitter-receiver sensor pairs are shifted and averaged according to the appropriate spatial rule to construct an image of the damage [18].

Multi-path effects due to boundaries of the medium make analyzing the wave propagation difficult. Delay-and-sum accounts for these multi-path effects and provides better resolution in image localization [35].

To implement delay-and sum, the inner product between the expected wave responses and measured wave responses is computed. Then, their sum is calculated across each receiver. Enveloped signal responses are typically used to avoid phase error. Enveloped responses refers to the absolute value of the analytic representation of the responses [35].

The traditional delay-and-sum requires sending an excitation signal to each sensor. The multi-delay-and-sum imaging algorithm [36] was proposed for damage detection in thin plate-like structures. Compared to the traditional delay-and-sum, the multi-delay-and-sum algorithm sends only one excitation signal for each detection.

Another method introduced to locate damage on isotropic structures is time reversal. Wang [37] proposed a synthetic time reversal method and successfully demonstrated detection of mass bonded on the plate.

1.2.2.2 Guided Wave Localization in Anisotropic Structures

Delay-and-sum imaging algorithms [34] have also been used for detecting damage in composites and has been effective for impact damage detection in composites [38]. Qiu [39] proposed a 2-step algorithm for damage detection and localization. In the first step, the damage area is identified by a damage index (DI) imaging algorithm. In step 2, the delay-and-sum algorithm is performed only in the area where damage is identified. The authors of [39] have shown successful detection of multiple damages in a composite wing panel.

The damage index refers to the value of the envelope of the baseline-subtracted signal at a time t_{ij} for all transducer paths ij, where i and j refer to a transmitter and receiver, respectively. The damage detection depends on the first mode reflected wave from the damage. The DI measurements are made focused on the first reflections from the damage and to ignore secondary reflections from the boundaries [38].

Time reversal methods are also used to detect damage in composites [40]. In [40], time reversal was applied to detect delamination in composite plate. For a relative plate of size 60.96 by 60.96 cm, 16 sensors were used, which amounts to 240 different measurements. This processing is very time consuming and computationally expensive [38].

To reduce the hardware requirements of the time reversal method, a modified time reversal method is introduced in [41]. This method successfully detected the presence and severity of impact damage in a composite plate.

1.2.3 Compressive Sensing and Sparsity

Compressive sensing [42, 43] is a signal processing framework that reconstructs a signal by using the fact that many signals are sparse, or mostly zeros, in nature. If a signal is sparse, in some basis, compressive sensing allows us to reconstruct or recover a signal from fewer measurements than traditionally possible.

In some applications, high sampling rate leads to large number of samples. As a result, data needs to be compressed for storage. The main idea behind compressive sensing is to directly sample a signal in a compressed form (low sampling rate), rather than first sampling using the Nyquist rate and then compressing it [44].

The principles of compressive sensing, such as sparsity, convex optimization, etc., are

used in channel coding to design fast error correcting codes [42], to protect from errors during transmission [45]. The requirements of compressive sensing are sparsity, which requires the signal to be sparse in some basis, and incoherence, which is applied through the isometric property [43].

Sparse recovery methods assume the relationship between the measured data $\mathbf{Y}$ and its sparse representation $\mathbf{V}$ are denoted by

$$\boldsymbol{Y} = \boldsymbol{\Phi} \boldsymbol{V}, \tag{1.2}$$

where $\mathbf{Y}$ is an M $\times$ Q matrix of measured data and $\mathbf{V}$ is an N $\times$ Q matrix of the sparse representation. In most cases, the linear operator $\boldsymbol{\Phi}$ is a matrix.

When the matrix $\boldsymbol{\Phi}$ is underdetermined, then there exists an infinite number of $\mathbf{V}$ matrices that satisfy the relationship in (1.2). Yet if $\mathbf{Y}$ is sparse and $\boldsymbol{\Phi}$ satisfies certain properties such as the restricted isometry property [46], then there exists algorithms that can uniquely recover $\mathbf{V}$ from the measured data $\mathbf{Y}$.

1.2.4 Sparse Wavenumber Analysis

A sparse recovery technique used to recover the frequency-wavenumber representation, or dispersion curves of the medium, from a set of measured data $\mathbf{Y}$ is called sparse wavenumber analysis [17]. We will be using a sparse wavenumber analysis to extract sparse representations of an anisotropic medium. Sparse wavenumber analysis recovers the sparse representation of the medium by considering the frequency-wavenumber representation of Lamb waves to be sparse.

In prior work, sparse wavenumber analysis has been used to accurately locate damage in an isotropic plate [20]. It has also been used to detect damage in pipelines under changing environmental and operational conditions [47].

For an isotropic plate, a Lamb wave between a transmitter and receiver at distance r and at angular frequency ω is modeled by

$$Y(\omega, r) = \sum_{n} \sqrt{\frac{1}{k_n(\omega) r}} G_n(\omega) e^{-j k_n(\omega) r}, \tag{1.3}$$

For mode n, $k_n(\omega)$ signifies the frequency-dependent wavenumber and is represented by a set of dispersion curves. These dispersion curves are shown in Figure 1.1 (b). The

dispersion curves of a medium describe how the wavenumber of a mode varies with frequency. The function $G_n(\omega)$ represents how the complex amplitude of the mode varies with frequency.

This model can be expressed as [14]

$$\boldsymbol{Y} = \boldsymbol{\Phi V}. \tag{1.4}$$

The M $\times$ Q matrix $\mathbf{Y}$ represents frequency-domain guided wave data, where Q is the number of frequencies and M is the number of measurements each corresponding to distance r. The N $\times$ Q matrix $\mathbf{V}$ represents wavenumber data where N is the number of wavenumbers. The M $\times$ N matrix $\mathbf{\Phi}$ represents the relationship between $\mathbf{Y}$ and $\mathbf{V}$ and is expressed by

$$\mathbf{\Phi} = [(k_n r_m)^{-1/2} e^{-jk_n r_m}]_{mn}. \tag{1.5}$$

The matrix $\mathbf{\Phi}$ describes how waves propagate within the medium.

In past work, a convex optimization technique known as basis pursuit denoising [48] was used to recover sparse representations of the medium from the measurements. The challenges faced in using basis pursuit were its slow implementation and dependency on a regularization parameter τ, whose value depends on the scenario and is generally unknown.

We will recover the sparse representation of an anisotropic system by using orthogonal matching pursuit [49]. In contrast with basis pursuit, orthogonal matching pursuit does not depend on regularization parameter τ. Also, implementation of orthogonal matching pursuit is faster than basis pursuit. Orthogonal matching pursuit will be discussed in detail in Chapter 2.

By using orthogonal matching pursuit, we can obtain the dispersion curve $\mathbf{V}$ of the medium from $\mathbf{Y}$.

1.2.5 Sparse Wavenumber Synthesis

Having obtained the frequency-wavenumber representation $\mathbf{V}$ of the medium, we can now find the Lamb wave response X (r, ω) between any two points in the medium. This is called sparse wavenumber synthesis. This is done by solving the forward equation (1.4).

Let the $\widehat{M}$ new distances be represented by $\widehat{r}_1, \widehat{r}_2, \ldots, \widehat{r}_{\widehat{M}}$. Using the dispersion curves $\mathbf{V}$ obtained from sparse wavenumber analysis, we want to estimate $\widehat{\mathbf{X}}$. This is implemented by solving

$$\widehat{\boldsymbol{X}} = \widehat{\boldsymbol{\Phi}}\boldsymbol{V}. \tag{1.6}$$

The matrix $\widehat{\Phi}$ has the same form as Φ used in (1.4), but with the new distances $\widehat{r}_1, \widehat{r}_2, \ldots,$ $\widehat{r}_{\widehat{M}}$. The matrix $\widehat{\mathbf{X}}$ represents the predicted measurements in the medium for each measurement.

1.2.6 Matched Field Processing

Matched field processing (MFP) is a model-based framework that is used to locate a target/scatterer/defect in a complex propagating environment. It is also referred to as a generalized beamforming framework [50], as the sensors need not be arranged in any particular order. MFP has been studied in non-destructive testing [20], seismology [51], and underwater acoustics [52]. It is also used in underwater acoustics to determine the unknown range and depth in an ocean environment [52].

We will use data-driven matched field processing [14], which is a framework that builds a model directly from measured data and then uses this model to locate defects. It is done by integrating matched field processing with a data-driven model obtained from sparse wavenumber analysis and sparse wavenumber synthesis.

Matched field processing compares measured baseline-subtracted data with the model data to localize a target. Measured baseline-subtracted data is obtained by subtracting the measured data without damage from data with damage. So, measured baseline-subtracted data refers to data from the transmitting sensor to the scatterer and then to the receiving sensor. Model data represents the estimated responses from the transmitter to the scatterer and then to the receiving sensor for $\mathbf{M}$ measurements. These $\mathbf{M}$ measurements correspond to a possible scatterer at different locations on the grid.

We integrate sparse wavenumber analysis with a coherent matched field processor and a sensor domain incoherent matched field processor. In Chapter 3, we apply coherent and sensor domain incoherent matched field processors to locate a scatterer on the composite plate.

1.3 Challenges

Composites are anisotropic in nature. That is, the waves in composites travel with different propagating speeds in different directions. Unlike in metals, there are not many well-defined wave propagation models for composites. Guided waves have been successfully used to detect and locate damage in many isotropic metals [16]. However, due to the anisotropic nature of many composites, traditional isotropic signal processing methods fail [18, 19]. This is partially due to not knowing the velocity characteristics of guided waves.

1.3.1 Solution

In this dissertation, we will use sparse wavenumber analysis [17] to determine the frequency-wavenumber (or phase velocity) characteristics of the guided waves in anisotropic composites from small sets of measurements.

There is no well-known closed-form solutions for how anisotropic waves propagate from a single point. This is because the solution must model an infinite number of possible wave velocities as a function of frequency and direction. Therefore, we create and use an approximate model for anisotropy in this thesis. This approach uses algorithms from compressive sensing to recover multimodal and dispersive properties (wavenumbers and complex amplitudes) of guided waves.

We use multidimensional multimodal and dispersive properties (which we will also refer to as dispersion curves) to predict how guided waves propagate in anisotropic plates through sparse wavenumber synthesis [17].

Finally, these predictions (i.e., a wave propagation model for the composites) are integrated with matched field processing [50], a model-based localization framework, to locate a transmitter source (e.g., a sensor) or a damage. We further expand and improve matched field processing to locate damage in an anisotropic plate by predicting guided wave behavior at any location in the structure.

1.4 Conclusion and Outline

In the following chapters, we recover the dispersion curves of a several composite plates and use them to locate damage. In Chapter 2, we derive our sparse wavenumber analysis and sparse wavenumber synthesis for anisotropic propagation. In Chapter 3, we

integrate the data-driven matched field processing with the model obtained from sparse wavenumber analysis and sparse wavenumber synthesis. In Chapter 4, we validate our model with different composite plates. In Chapter 5, we include future work that can be done on our model.

CHAPTER 2

SPARSE WAVENUMBER ANALYSIS AND SYNTHESIS IN COMPOSITES

2.1 Motivation

Detecting and locating damage in a structure relies on the ability to characterize guided wave behavior accurately. Guided waves exhibit multimodal and dispersive behavior while propagating in a structure. That is, the waves consist of different wave modes, with each mode travelling with a frequency-dependent velocity. The velocity of the waves is also affected by environmental variations. Moreover, the waves may also experience reflections from the boundaries of the structure. All this leads to difficulty in characterizing and analyzing guided waves and hence, makes it difficult to detect damage in a structure.

In prior work, sparse wavenumber analysis [17], a signal processing technique, has been introduced to recover the multimodal and dispersive properties of guided waves. Sparse wavenumber analysis is based on compressive sensing [42, 43]. Compressive sensing recovers sparse signals (a signal containing mostly zeros) efficiently through the use of sparse recovery algorithms. We use compressive sensing combined with the fact that Lamb waves are sparse in the frequency-wavenumber domain to recover the frequency-wavenumber representation of Lamb waves accurately with a fewer number of sensors than the traditional methods, such as two-dimensional discrete Fourier Transform (2D-DFT) [53], various time-domain matching pursuit [54] and time-frequency analysis methods [55, 56]. The time-domain matching pursuit and time-frequency analysis methods require only one set of measurements. However, these methods cannot obtain the useful phase information of the waves as sparse wavenumber analysis does.

In prior work, sparse wavenumber analysis has been applied to isotropic media. In Section 2.2, we create a sparse wavenumber analysis technique for an anisotropic medium. We review orthogonal matching pursuit, which we use to solve the Lamb wave inverse

problem. In Section 2.3, we show how sparse wavenumber synthesis can be used to successfully predict the wave response between any two points on the plate. In Section 2.4, we discuss our experimental methodology, where we have used 11 ultrasonic transducers arranged in a random order across a unidirectional composite plate. In Section 2.5, we experimentally show that sparse wavenumber analysis accurately recovers the frequency-wavenumber representation of Lamb waves and predicts the corresponding wave fields.

We show that these predicted responses and the measured responses can achieve correlation coefficients greater than 0.60.

2.2 Sparse Wavenumber Analysis

Anisotropic materials, such as fiber reinforced composites, are difficult to analyze because Lamb waves in anisotropic media travel with different velocities in different directions. The typical signal representation between any two sensors in an isotropic medium is given by

$$Y(\omega, r) = \sum_n \sqrt{\frac{1}{k_n(\omega) r}} G_n(\omega) e^{-j k_n(\omega) r}, \tag{2.1}$$

where r is the distance between the two sensors.

The expression in (2.1) states that the wave travels in all directions as a sum of wave modes with frequency-dependent wavenumber $k_n(\omega)$ and a single distance r. The frequency-dependent wavenumber $k_n(\omega)$ is inversely proportional to phase velocity and therefore describes the wave speed in all directions across the medium. The complex amplitude of the mode n is represented by $G_n(\omega)$.

Yet, due to direction-dependent velocities in composites, the isotropic signal representation is not valid. In fact, while there are analytical solutions for how anisotropic waves propagate as a plane wave [57], there is no well-known closed-form solutions for how anisotropic waves propagate from a single point. This is because the solution must model an infinite number of possible wave velocities as a function of frequency and direction. Therefore, we create and use an approximate model for anisotrophy in this thesis. Specifically, sparse wavenumber analysis is performed by characterizing the propagation direction of waves based on horizontal and vertical wavenumber. We model these waves according to

$$Y(\omega, x, y) = \sum_n G_n(\omega) e^{-j[(k_n^x(\omega)x)^{P0} + (k_n^y(\omega)y)^{P0}]^{\frac{1}{P0}}}, \tag{2.2}$$

$G_n(\omega)$ represents how the complex amplitude of the mode n varies with frequency. Distance of wave propagation in the horizontal direction and vertical direction is represented by x and y, respectively. The variables k_n^x and k_n^y denote the wavenumbers of the waves in the horizontal and vertical direction, respectively, for a mode n.

While the model only requires the knowledge of two wavenumber functions in orthogonal directions, the function actually defines all velocities between those directions. The velocities are defined by the $P0$ variable. $P0$ is a shape factor for a mode n. It describes the shape of the wave front (the shape of velocity surface). $P0 = 2$ describes an elliptical phase velocity of guided waves with reference to the direction of propagation. This can be shown mathematically. The wavenumber $k_n^x(\omega)$ and $k_n^y(\omega)$ of each mode n in (2.2) can be defined as a function of propagation direction θ and distance $x = \cos\theta$ and $y = \sin\theta$. We get

$$k_n'(\omega, \theta) = [(k_n^x(\omega)\cos\theta)^{P0} + (k_n^y(\omega)\sin\theta)^{P0}]^{\frac{1}{P0}}. \tag{2.3}$$

The wave propagation model defined in (2.2) assumes that the waves are travelling in an outward direction with a frequency-dependent phase velocity [58], where phase velocity $v_n(\omega, \theta) = \omega / k_n'(\omega, \theta)$ is represented by

$$v_n(\omega, \theta) = \omega[(k_n^x(\omega)\cos\theta)^{P0} + (k_n^y(\omega)\sin\theta)^{P0}]^{\frac{-1}{P0}}]. \tag{2.4}$$

For $P0 = 2$, (2.4) gives the equation for an ellipse, where $\omega[k_n^x(\omega)]^{-1}$ and $\omega[k_n^y(\omega)]^{-1}$ are the magnitudes in horizontal and vertical direction, respectively.

By changing $P0$, the shape of the phase velocity surface changes. As $P0$ decreases, the corners of the velocity surface compress inwards and as $P0$ increases, the corners expand outwards [20], as seen in Figure 2.1.

Sparse wavenumber analysis assumes the relationship between the measured data $\mathbf{Y}$ and its sparse representation $\mathbf{V}$ is [20]

$$\boldsymbol{Y} = \boldsymbol{\Phi V}, \tag{2.5}$$

The matrix $(M \times Q)$ $\mathbf{Y}$ represents frequency-domain guided wave data, where Q is the number of frequencies and M is the number of measurements, with corresponding

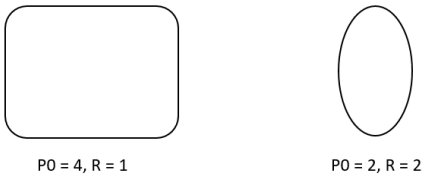

Figure 2.1. Shape of phase velocity surfaces for two different values of $P0$ (shape factor) and R (where $R = \frac{k_n^x(\omega)}{k_n^y(\omega)}$).

distance in horizontal direction x and vertical direction y. The N $\times$ Q matrix $\mathbf{V}$ represents wavenumber data where N is the number of wavenumbers. In an anisotropic medium, the matrix Φ of size M $\times$ N represents the relationship between $\mathbf{Y}$ and $\mathbf{V}$ and is expressed by

$$\mathbf{\Phi} = e^{-j[(k_n^x(\omega)x)^{P0} + (k_n^y(\omega)y)^{P0}]^{\frac{1}{P0}}}. \tag{2.6}$$

The matrix Φ describes how waves propagate within the medium. In the next section, we describe how to recover the sparse matrix $\mathbf{V}$ from our data $\mathbf{Y}$.

2.2.1 Sparse Recovery Algorithm: Orthogonal Matching Pursuit

To recover the sparse representation of a signal, we will be using orthogonal matching pursuit. In past work, a convex optimization technique known as basis pursuit denoising [48] was used to recover sparse representations of the medium from the measurements. The challenges faced in using basis pursuit were its slow implementation and dependency on a regularization parameter τ, whose value depends on the scenario and is generally unknown.

The sparse recovery algorithm that we will use to recover the sparse representation of an anisotropic system is orthogonal matching pursuit [49]. In contrast with basis pursuit, orthogonal matching pursuit does not depend on regularization parameter τ. Also, implementation of orthogonal matching pursuit is faster than basis pursuit.

Orthogonal matching pursuit is a greedy, iterative algorithm and is implemented by performing the following steps.

2.2.1.1 Step I

The inner product of $\Phi^H \mathbf{y}_q$ finds the best column/atom of matrix Φ that matches the measured data $\mathbf{y}_q$, where $1 \leq q \leq Q$ frequencies.

2.2.1.2 Step II

$$B \leftarrow B \cup \arg\max_i |\Phi_i^H \mathbf{y}_q| \tag{2.7}$$

The set B of indices is obtained by finding the index of Φ belonging to the maximum value of inner product of $\Phi^H \mathbf{y}_q$. That is, B represents a set of indics corresponding to the atoms of Φ that we use in our algorithm.

2.2.1.3 Step III

Matrix Φ_B consists of columns of Φ corresponding to indices defined in B. This best matching set of columns/atoms is fit to $\mathbf{y}_q$ in least square sense and is subtracted from $\mathbf{y}_q$ such that.

$$\widehat{\mathbf{v}}_q \leftarrow \arg\min_{\mathbf{v}_q} \left\| \mathbf{y}_q - \Phi_B \mathbf{v}_q \right\|_2^2 \tag{2.8}$$

$$\mathbf{y}_q \leftarrow \mathbf{y}_q - \Phi_B \, \widehat{\mathbf{v}}_q \tag{2.9}$$

2.2.1.4 Step IV

The above steps are repeated until the desired sparsity (i.e., number of non-zeros values) is achieved.

2.3 Sparse Wavenumber Synthesis

Having obtained the frequency-wavenumber representation $\mathbf{V}$ (also known as the dispersion curves) of the medium, we can now find the Lamb wave response $X(x, y, \omega)$ between any two points in the medium. This process is called sparse wavenumber synthesis. This is done by solving the forward equation (2.5).

Using the dispersion curve $\mathbf{V}$ obtained from sparse wavenumber analysis, we want to estimate $\widehat{\mathbf{X}}$. This is implemented by solving

$$\widehat{X} = \widehat{\Phi} V. \tag{2.10}$$

$\widehat{\Phi}$ has the same form as Φ used in (2.6) but with new distances in horizontal directions $\widehat{x}_1$, $\widehat{x}_2$,...,$\widehat{x}_M$ and vertical directions $\widehat{y}_1$, $\widehat{y}_2$,...,$\widehat{y}_M$.

2.4 Experimental Methodologies

We test our sparse wavenumber analysis and sparse wavenumber synthesis on a 1.20 m $\times$ 1.17 m $\times$ 0.002 m carbon-fiber unidirectional composite plate. A unidirectional composite plate has all of the fibers aligned in one direction. To transmit and receive Lamb wave signals, we attached eleven PZT transducers randomly across the top surface of the plate. Sensors are placed randomly on the plate so as to have minimum correlation between measurements (a requirement of compressive sensing) and also so that no bias affects the result. The total number of unique measurements obtained is 55, according to $\frac{N(N-1)}{2}$, where N is the number of sensors on the plate.

2.4.1 Data Collection

We collect baseline calibration data without damage on the plate by transmitting and measuring a 5 μs linear chirp from 50 kHz to 600 kHz between each pair of transducers. This will result in 55 unique measurements across each pair of sensors. This baseline data is used to compare with data obtained from the damaged plate.

In Figure 2.2, each square indicates a sensor used to transmit and receive signals and the bold circle indicates the location of the scatterer. Then, we collect the data again by placing a scatterer, simulating damage, on the plate. In our experiment, we place a metal cuboid of size approximately 3.302 cm $\times$ 2.794 cm $\times$ 1.651 cm on the plate to act as a scatterer and collected an additional 55 measurements in the same manner. The scatterer is shown in Figure 2.3. Baseline subtraction is accomplished by subtracting the measured data without the scatterer from measured data with the scatterer. The remaining data should consist of only the scattered signal.

2.5 Experimental Results

We tested our methodology with experimental data collected using 11 sensors. In this section, we demonstrated the results from three different tests.

(1) We recover the dispersion curve in the frequency-wavenumber domain using sparse wavenumber analysis.

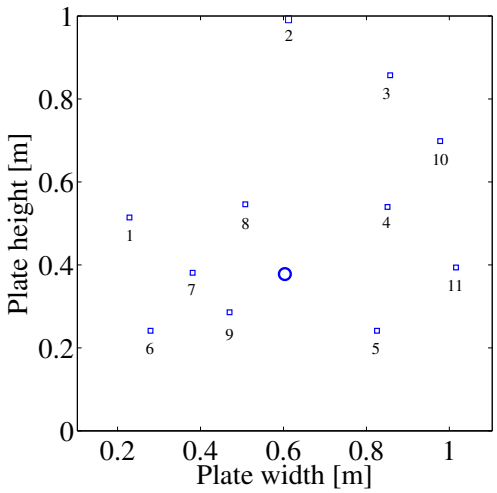

Figure 2.2. Illustration of unidirectional carbon fiber composite plate used for our experimental setup. Each square represents a transducer and bold circle represents the scatterer (mass).

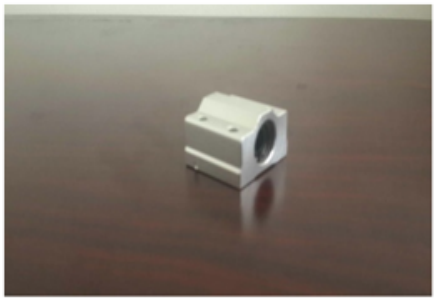

Figure 2.3. The scatterer used in the experiments.

(2) We use the dispersion curves obtained to predict the Lamb wave response between two points on the plate using sparse wavenumber synthesis.

(3) We use dispersion curves to predict the entire wavefield across the plate.

2.5.1 Sparse Wavenumber Analysis

The frequency-wavenumber representation of Lamb waves (dispersion curves) for a single mode is shown in Figure 2.4. We discretized the horizontal wavenumber space uniformly across 801 samples and vertical wavenumber space uniformly across 501 samples. This figure illustrates how the vertical wavenumber k_y and horizontal wavenumber k_x, varies as a function of frequency. The horizontal wavenumber, k_x, represents waves

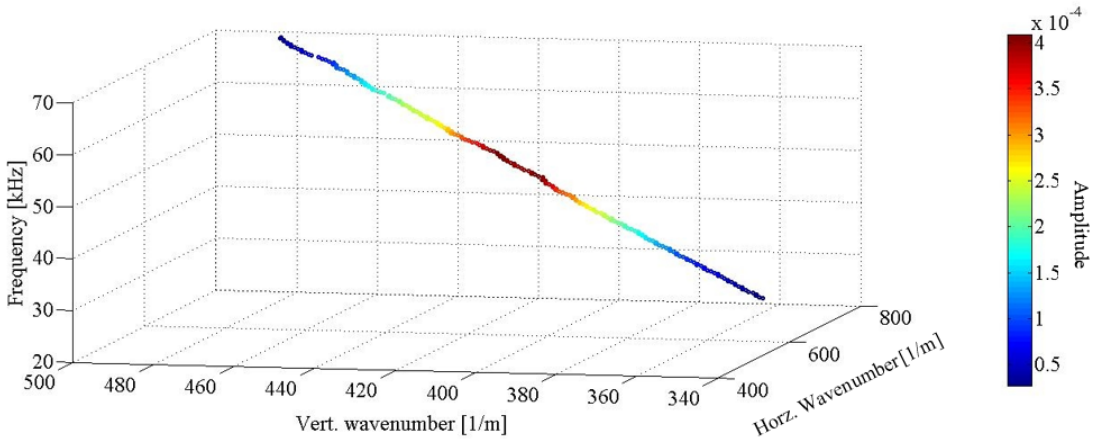

Figure 2.4. Dispersion curve of a unidirectional composite plate recovered using sparse wavenumber analysis.

traveling in horizontal direction, that is, in the direction perpendicular to the fibers. The vertical wavenumber k_x represents waves traveling in vertical direction, that is, in the direction parallel to the fibers.

Each non-zero component in Figure 2.4 gives the value of horizontal and vertical wavenumber. The corresponding value at each location gives the amplitude. In the frequency range of 45 kHz to 50 kHz, the amplitude of the waves is maximum. For 50 kHz frequency, the horizontal and vertical wave numbers are 680 and 417, respectively. As phase velocity is inversely proportional to the wave numbers, higher wavenumber denotes slow phase velocity. Hence, the dispersion curve shows that waves are moving faster in the vertical direction and slower in horizontal direction.

2.5.2 Sparse Wavenumber Synthesis

Figure 2.5(a) and Figure 2.5(b) show measurements taken from the composite plate at two different points and compare them with the reconstructed measurements obtained from sparse wavenumber synthesis. Specifically, sparse wavenumber synthesis is used to synthesize the signal response between sensor pair $(2, 8)$ and $(3, 11)$. Figure 2.2 shows the locations and labels of these sensors. Figure 2.5(a) and Figure 2.5(b) show that our reconstructed signal matches the measured signal response, but not completely. There is partial overlap between the measured signal and reconstructed signal. The synthesized

(a)

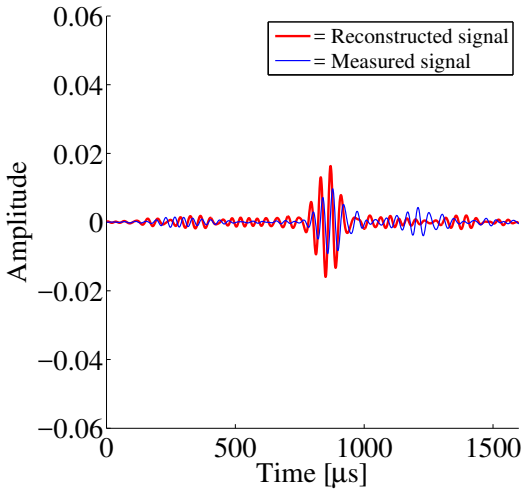

(b)

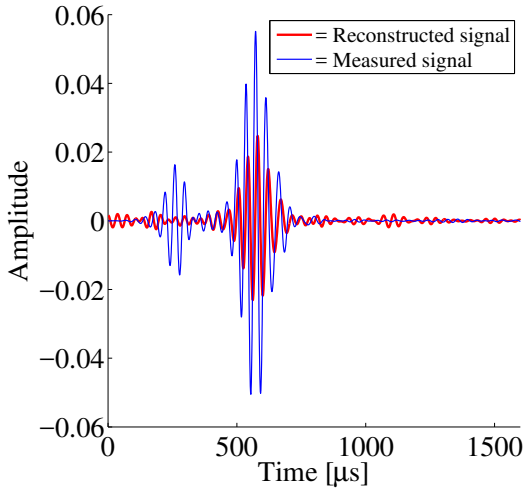

Figure 2.5. The blue signal shows the measured signal and the red one shows the reconstructed signal using sparse wavenumber synthesis. (a) second sensor as transmitter and eighth sensor as receiver, (b) third sensor as transmitter and eleventh sensor as receiver (sensor numbers are specified according Figure 2.2).

measurement between sensor 2 and sensor 8 has a correlation coefficient of around 0.20 with measured signal path, whereas the synthesized measurement between sensor 3 and sensor 11 has a correlation coefficient of around 0.26 with measured signal. This demonstrates that our model can be further improved. This partial overlap allows us to locate the scatterer properly.

Figure 2.5(a) shows an effective S0 mode (at time around 300 ms) and an effective A0 mode (at time around 800 ms). The reconstructed wave appears to fit the A0 mode but fails to reconstruct the S0 mode properly. This is likely due to the A0 mode being much

stronger in the data. Figure 2.5(b) shows the effective S0 mode (at time around 250 ms) and effective A0 mode (at time around 600 ms). The reconstructed wave again appears to fit the A0 mode but fails to reconstruct the S0 mode. In Figure 2.5, there is a slight shift between the reconstructed and measured signal. One of the reasons may be due to error in our model.

2.5.3 Wavefields

The dispersion curves obtained using sparse wavenumber analysis are used to predict the full wavefields. Figure 2.6 shows the wavefield at 4 different time intervals, starting from (a) to (d). We observe from Figure 2.6 that the outermost wave propagation is the S0 mode, followed by the A0 mode. Also, the shape of wavefield is mostly elliptical, which corresponds to the the shape that we obtained using P0 value of 1.8627 in Section 2.2. We can also see that the major axis of the ellipse is along the plate length, and the minor axis is along the plate width.

We can observe from the wave fields that waves are propagating faster in the vertical direction, that is, in the direction along the fibers. Hence, our conclusion in Section 2.5.1 is validated by the wave fields obtained.

2.6 Conclusion

In this chapter, we have taken advantage of sparse representations to predict the behavior of guided waves in a complex environment. We have used sparse wavenumber analysis to recover dispersion curve of waves in a composite plate and these dispersion curves closely represent theoretical dispersion curves. Then, we estimated the wave behavior in the entire plate medium by using sparse wavenumber synthesis.

We tested our methodology on a unidirectional composite plate with 11 sensors placed in random locations. We accurately recovered the dispersion curve (frequency-wavenumber representation) using sparse wavenumber analysis. We then use this representation to predict Lamb wave response between any two points on the plate.

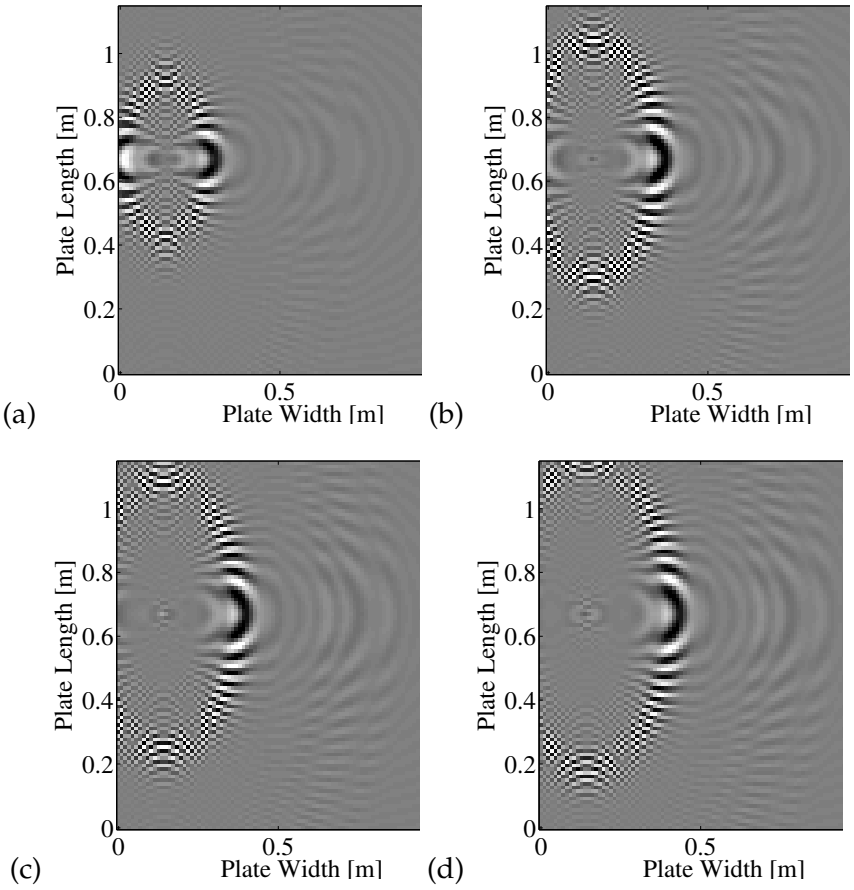

Figure 2.6. Wavefields at 4 instances (a) Wavefield at 200 samples, (b) wavefield at 300 samples, (c) wavefield at 350 samples, and (d) wavefield at 400 samples.

CHAPTER 3

DATA-DRIVEN MATCHED FIELD PROCESSING

3.1 Motivation

Matched field processing is a generalized model-based framework that is used to locate damage in a complex propagating environment. It has been used in seismology [51], non-destructive evaluation [20], and underwater acoustics [52]. Due to the multimodal and dispersive characteristics of guided waves, matched field processing is an attractive tool to locate damage with guided wave structural health monitoring.

Data-driven matched field processing is a framework that builds multimodal propagation models of the propagating environment from the measured data and then uses this model to locate damage in a structure. In prior work [50], data-driven matched field processing has been used to detect damage on an aluminum plate. We expand this approach to locate damage on composite structures by taking into account the anisotropic nature of composites. We build a model directly from measured data using sparse wavenumber analysis and sparse wavenumber synthesis. This model is referred to as a sparsity-based data-driven model [50], as it is built from sparse representations of measured data (which is recovered using compressive sensing). Finally, this data-driven model is integrated with matched field processing to locate damage on a structure.

Our method allows us to use all wave modes and dispersion characteristics of guided waves to detect damage on the composite plate with high accuracy and resolution. We perform sparse wavenumber analysis using orthogonal matching pursuit [49], which is a greedy iterative algorithm.

In this chapter, we construct a data-driven model using sparse wavenumber analysis and sparse wavenumber synthesis and integrate it with matched field processing. We integrate the data-driven model using a coherent matched field processor [50] and sensor

domain incoherent matched field processor. We demonstrate the validity of our methodology by localizing a scatterer on a unidirectional carbon-fiber and a glass-fiber composite plate. We compare our data-driven matched field processing with a delay-and-sum-based approach [35], a commonly used technique in structural health monitoring.

3.2 Data Collection

To implement data-driven matched field processing, we take into account three data sets: measured data, baseline-subtracted data, and model data. The measured data represents the wave measurements between each pair of sensors. The baseline-subtracted data represents the wave measurements between each pair of sensors through the scatterer. The model data represents the synthesized measurements obtained using sparse wavenumber synthesis, which predicts what the data will look like if the scatterer is placed at a given location.

3.2.1 Measured Data

The measured data is represented by a matrix $\mathbf{Y}$ of size $M \times Q$, where M is the number of measurements and Q is the number of discrete frequencies $\omega_1, \omega_2, ..., \omega_Q$. Each column of $\mathbf{Y}$ represented by

$$\mathbf{y}_q = [Y(\omega_q, 1), \ldots, Y(\omega_q, M)]^T + \mathbf{n}_q, \tag{3.1}$$

where $\mathbf{y}_q$ is $M \times 1$ vector and $\mathbf{n}_q$ is the error due to noise at the ω_q frequency. Measured data represents the signal transmitted and received between each sensor pair with known measurements $m = 1, \ldots, M$.

3.2.2 Baseline-Subtracted Data

The baseline-subtracted data is represented by a matrix $\mathbf{X}$ of size M $\times$ Q, where M is the number of measurements and Q is the number of discrete frequencies $\omega_1, \omega_2, ..., \omega_Q$. Each column of $\mathbf{X}$ represented by

$$\mathbf{x}_q = [X(\omega_q, 1), \ldots, X(\omega_q, M]^T + \mathbf{n}_q, \tag{3.2}$$

where $\mathbf{x}_q$ is a M $\times$ 1 vector and $\mathbf{n}_q$ is the error due to noise at the ω_q frequency. The baseline-subtracted data represents the signal (for $1 \leq m \leq M$) from the transmitter to the scatterer and then from the scatterer to the receiving sensor. This is obtained by removing

the baseline information, that is, by taking the wave measurements without the scatterer and subtracting them from the wave measurements with the scatterer on the plate.

3.2.3 Model Data

The model data is represented by $\widehat{\mathbf{X}}$ of size M $\times$ Q, where M is the number of measurements and Q is the number of discrete frequencies $\omega_1, \omega_2, \ldots, \omega_Q$. Each column of $\widehat{\mathbf{X}}$ represented by

$$\widehat{\mathbf{x}}_q = [\widehat{X}(\omega_q, 1, \mathbf{r}), \ldots, \widehat{X}(\omega_q, M, \mathbf{r})]^T, \tag{3.3}$$

where $\widehat{\mathbf{x}}_q$ is a M $\times$ 1 vector at ω_q frequency. $\widehat{\mathbf{X}}$ represents the estimated responses of $\mathbf{X}$. The data for measurement m represents guided waves travelling from the transmitting sensor to the scatterer (at coordinate $\mathbf{r} = [x_s, y_s]$) and then to the receiving sensor, with the scatterer placed at a given location. The baseline subtraction process is illustrated in Figure 3.1 for the isotropic scenario and in Figure 3.2 for the anisotropic scenario.

For the isotropic case, the baseline subtracted signal (Figure 3.1) is modelled by

$$\widehat{X}(\omega, m, \mathbf{r}) = \sum_n \sqrt{\frac{1}{k_n(\omega) r}} G_n(\omega) e^{-j k_n(\omega)(r_{1,m} + r_{2,m})}. \tag{3.4}$$

In contrast with (2.1), this model incorporates both the travel distance from the transmitter to the damage $r_{1,m}$ and the travel distance from the damage to the receiver $r_{2,m}$. Our proposed model considers the wave path for each mode from the transmitter to the scatterer as a separate linear system than the wave path from the scatterer to the receiver. Therefore, the total wave path length is the combined path length between the transmitter and the scatterer and the scatterer to the receiver. Equivalently, the corresponding impulse response for each mode is given by the convolution of the impulse response between the transmitter and the scatterer with the impulse response between the damage and the receiver for each mode. Therefore, using the property that convolution in time is multiplication in frequency, the baseline signal is modelled as (3.4).

For the anisotropic case, the baseline subtracted signal (Figure 3.2) is modelled by

$$\widehat{X}(\omega, m) = \sum_n G_n(\omega) e^{-j[(k_n^x(\omega) x_{1,m})^{P0} + (k_n^y(\omega) y_{1,m})^{P0}]^{\frac{1}{P0}} + [(k_n^x(\omega) x_{2,m})^{P0} + (k_n^y(\omega) y_{2,m})^{P0}]^{\frac{1}{P0}}}. \tag{3.5}$$

In contrast with (2.2), this model incorporates both the travel distance from the transmitter to the damage in the horizontal and vertical directions $x_{1,m}$ and $y_{1,m}$, respectively, and the

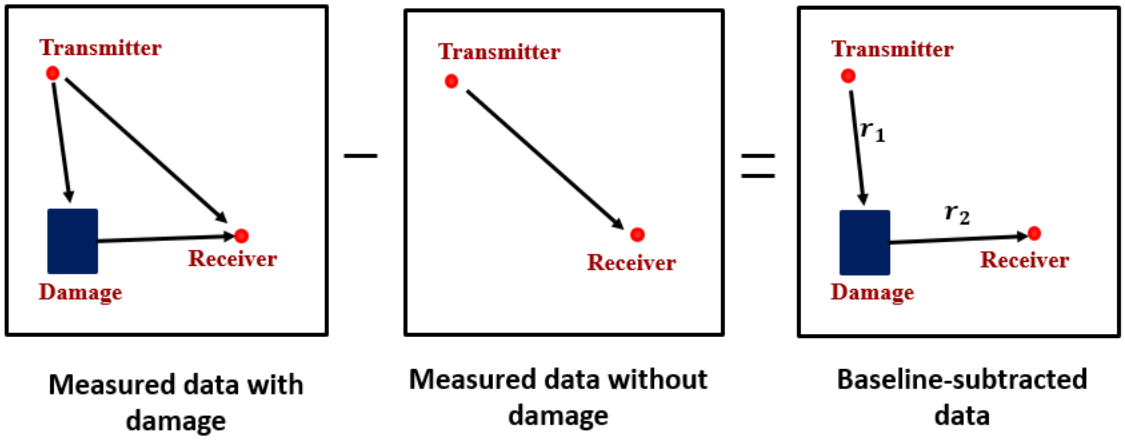

Figure 3.1. Illustration of baseline subtracted data for an isotropic medium

travel distance from the damage to the receiver in the horizontal and vertical directions $x_{2,m}$ and $y_{2,m}$, respectively. As the waves in composite travel in different velocities, at an instance of time, distance travelled in the horizontal direction is different from distance travelled in the vertical direction. Therefore, we incorporate horizontal and vertical distances in our model.

Our model proposes that total wave path is the convolution of two systems for each mode, with one system describing wave path from transmitter to scatterer and the other system describing wave path from scatterer to receiver. Since the wave path between two points in an anisotropic medium is modelled by (2.2), our output baseline-subtracted signal is modelled by (3.5).

3.3 Data-Driven Matched Field Processing

In this section, we implement data-driven matched field processing by integrating the data-driven model obtained from sparse wavenumber analysis and sparse wavenumber synthesis with matched field processing. We assume our sensors are placed in a random order on the plate.

Matched field processing compares measured baseline-subtracted data with the model data (shown in Figure 3.3) to localize a target. Measured baseline-subtracted data refers to data from the transmitting sensor to the scatterer and then to the receiving sensor. Model data represents the estimated responses from the transmitter to the scatterer and then to the

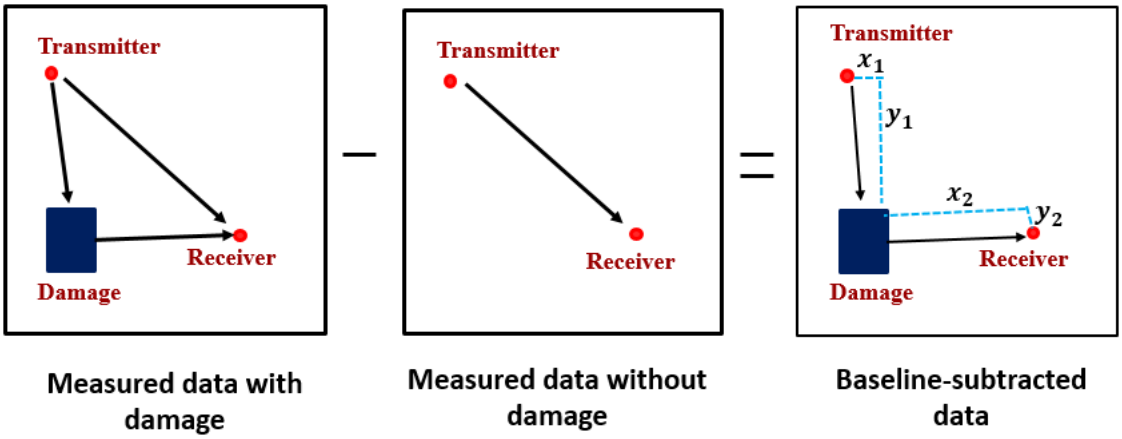

Figure 3.2. Illustration of baseline subtracted data for an anisotropic medium

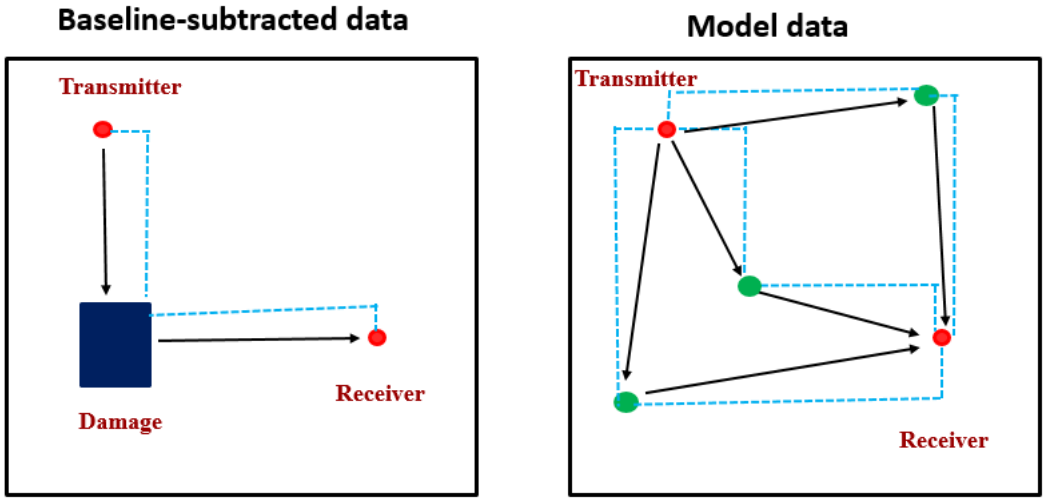

Figure 3.3. Illustration of matched field processing. Green circles represent possible scatterer at different locations on the grid. Blue dotted lines represent the horizontal and vertical distances from transmitter to possible scatterer and from possible scatterer to receiver.

receiving sensor for M measurements. These M measurements correspond to a possible scatterer at one location on the grid. Then, we model these M measurements for each possible scatterer location.

To obtain the data-driven model, we use sparse wavenumber analysis and sparse wave number synthesis. Sparse wavenumber analysis uses algorithm from compressive sensing [44] to recover sparse representation of guided waves in frequency-wavenumber domain

V. Figure 2.4 illustrates the dispersion curves which are obtained using sparse wavenumber analysis. Then, sparse wavenumber synthesis uses these recovered dispersion curves **V** to predict how waves propagate between points on the plate.

3.3.1 The Data-Driven model

Sparse wavenumber analysis recovers the frequency-wavenumber representation of the medium (or dispersion curves) by orthogonal matching pursuit, a greedy iterative algorithm. Then, using these recovered frequency-wavenumber representations, we create data-driven model data of the medium using sparse wavenumber synthesis by solving the forward equation

$$\widehat{\mathbf{x}}_q = \widehat{\Phi}\mathbf{v}_q, \tag{3.6}$$

$\widehat{\mathbf{x}}_q$ represents the predicted wave response between any two points in the medium. The matrix $\widehat{\Phi}$ used to create the model is defined as

$$\widehat{\Phi} = \left[e^{-j[[(k_n^x(\omega)x_{1,m})^{p0}+(k_n^y(\omega)y_{1,m})^{p0}]^{\frac{1}{p0}}+[(k_n^x(\omega)x_{2,m})^{p0}+(k_n^y(\omega)y_{2,m})^{p0}]^{\frac{1}{p0}}}\right]_{mn}. \tag{3.7}$$

Here, $x_{1,m}$ and $x_{2,m}$ represent the horizontal distance between the scatterer and the transmitter and the horizontal distance between the scatterer and the receiver, respectively. In the vertical direction, distance between the scatterer and the transmitter and distance between the scatterer and the receiver is represented by $y_{1,m}$ and $y_{2,m}$, respectively.

3.3.2 Coherent Matched Field Processor

A coherent matched field processor [59] is a widely used matched field processor. The coherent matched field processor is represented by the inner product between baseline-subtracted data **X** and model data $\widehat{\mathbf{X}}$. In this section, we integrate our data-driven model obtained in (3.6) with the coherent matched field processor.

The output of a matched field processor is an ambiguity surface that represents discretized locations on the plate with their source localization value. The larger the source localization value, the more closely matched is the data and model.

Estimated location $\widehat{\mathbf{r}}$ of a scatterer is defined as

$$\widehat{\mathbf{r}} = \arg\max_{\mathbf{r}} b(\mathbf{r}),$$

where $\mathbf{r}$ is a vector of coordinates. The ambiguity function of a coherent matched field processor can be obtained by solving the following least-square optimization [20, 59]

$$\widehat{\mathbf{r}} = \arg\min_{\mathbf{r},\beta} \sum_{m=1}^{M} \sum_{q=1}^{Q} |X(\omega_q, m) - \beta \widehat{X}(\omega_q, m, \mathbf{r})|^2. \tag{3.8}$$

Here, $X(\omega_q, m)$ represents the measured baseline-subtracted data (data with scatterer minus the data without scatterer), and $\widehat{X}(\omega_q, m, \mathbf{r})$ represents the model data (obtained from sparse wavenumber synthesis) for sensor m at frequency q. The variable β is the complex-valued, unknown amplitude of measured signal.

By solving for β, the coherent matched field processor can be expressed as a maximization problem [20], and its ambiguity function is expressed as

$$b(\mathbf{r}) = \frac{|\sum_{m=1}^{M} \sum_{q=1}^{Q} X(\omega_q, m) \widehat{X}(\omega_q, m, \mathbf{r})|^2}{\sum_{m=1}^{M} \sum_{q=1}^{Q} |\widehat{X}(\omega_q, m, \mathbf{r})|^2}. \tag{3.9}$$

The coherent matched field processor uses all of the phase information of the signals for scatterer localization. This creates noisy subbands but gives high resolution.

3.3.3 Sensor Domain Incoherent Matched Field Processor

In this section, we integrate our data driven model in (3.4) with a sensor domain incoherent matched field processor to localize a scatterer. As defined before, the estimated location $\widehat{\mathbf{r}}$ of a scatterer is given by

$$\widehat{\mathbf{r}} = \arg\max_{\mathbf{r}} b(\mathbf{r}).$$

The ambiguity function of a sensor domain incoherent matched field processor can be obtained by solving the following optimization problem [20, 59].

$$\widehat{\mathbf{r}} = \arg\min_{r,\beta_1,\ldots,\beta_M} \sum_{m=1}^{M} \sum_{q=1}^{Q} |X(\omega_q, m) - \beta_m \widehat{X}(\omega_q, m, \mathbf{r})|^2. \tag{3.10}$$

Here, $X(\omega_q, m)$ represents the measured baseline-subtracted data given in (3.2), and $\widehat{X}(\omega_q, m, \mathbf{r})$ represents the model data given in (3.3) for sensor m at frequency q. Instead of using a single constant β, as used in a coherent matched field processor, we use a different value at each measurement, given by β_m.

By solving for β_m, a sensor domain incoherent matched field processor can be expressed as a maximization problem [20], and its ambiguity function is expressed as

$$b(\mathbf{r}) = \sum_{m=1}^{M} \frac{|\sum_{q=1}^{Q} X(\omega_q, m)\widehat{X}(\omega_q, m, \mathbf{r})|^2}{\sum_{q=1}^{Q} |\widehat{X}(\omega_q, m, \mathbf{r})|^2}. \tag{3.11}$$

The sensor domain incoherent matched field processor takes the phase difference between the frequencies but ignores the phase difference between sensor pairs to localize a scatterer. This creates robustness to differences between sensor impulse responses but reduces the overall resolution.

3.4 Results

The measured baseline-subtracted data and model data is passed through a matched field processor to localize the scatterer. We use the same experimental setup described in Chapter 2 and shown in Figure 2.3. The result, or image, from the matched field processor is known as an ambiguity surface.

3.4.1 Carbon Fiber Composite Plate

For a unidirectional carbon fiber composite plate, the results are as follows. Figure 3.4 illustrates the magnitude of two ambiguity surfaces for two different pairs of sensors. Large values in the ambiguity surface indicate areas of likely damage.

Figure 3.4(a) illustrates the result for sensors 2 and 8 and Figure 3.4(b) illustrates the result for sensors 3 and 11, as indicated in Figure 2.2. The bold circle in Figures 3.4 and 3.5 indicates the scatterer. The final ambiguity surfaces are computed using (3.8) and (3.9). Figure 3.5 (a) illustrates the result with the coherent matched field processor in (3.8). Figure 3.5 (b) illustrates the result with the sensor domain incoherent matched field processor in (3.9).

The coherent matched field processor takes into account all of the phase information to localize a scatterer. As a result, this leads to destructive and constructive interference patterns, as shown in Figure 3.5 (a). This makes the coherent matched field processor sensitive to errors. Yet the resolution of the coherent matched field processor is high when compared to the sensor domain incoherent matched field processor, as seen in Figure 3.5. Figure 3.5 (b) shows a matched field processor in which phase difference between each sensor pair is not taken into consideration but phase difference across frequencies is used. As a result, the sensor domain incoherent matched field processor has high robustness to

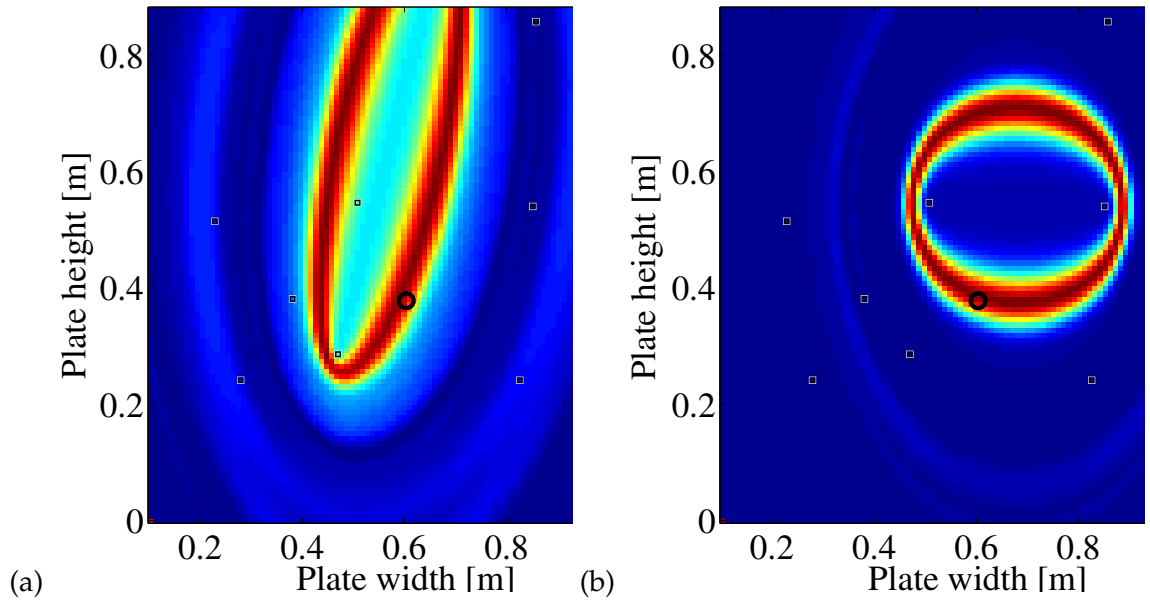

Figure 3.4. Damage detection by (a) sensor pair 2 and 8 and (b) sensor pair 3 and 11 (according to sensor orientation given in Figure 2.2).

errors between sensors. We compare our data-driven approach with a commonly used method for damage detection called delay-and-sum. This technique uses a single mode model with constant and equal phase and group velocities. The delay-and-sum does not successfully localize the scatterer on a carbon-fiber composite plate as shown in Figure 3.6.

3.4.2 Glass-Fiber Composite Plate

We tested our algorithm by successfully localizing damage on a 0.635 m $\times$ 0.635 cm $\times$ 0.005 m glass-fiber composite plate. Similar to Figure 2.2, Figure 3.7 shows the sensor orientation for 13 sensors on the glass-fiber composite plate, with the bold circle representing the scatterer (Figure 2.3).

The final ambiguity surfaces for the glass-fiber composite plate are shown in Figure 3.8. We can observe from the images that the matched field processors locate the scatterer in the glass-fiber composite plate but there is noise in the image. One of the reasons might be that our model is not perfect. The delay-and-sum method does not localize the scatterer in the glass-fiber composite plate, as shown in Figure 3.9.

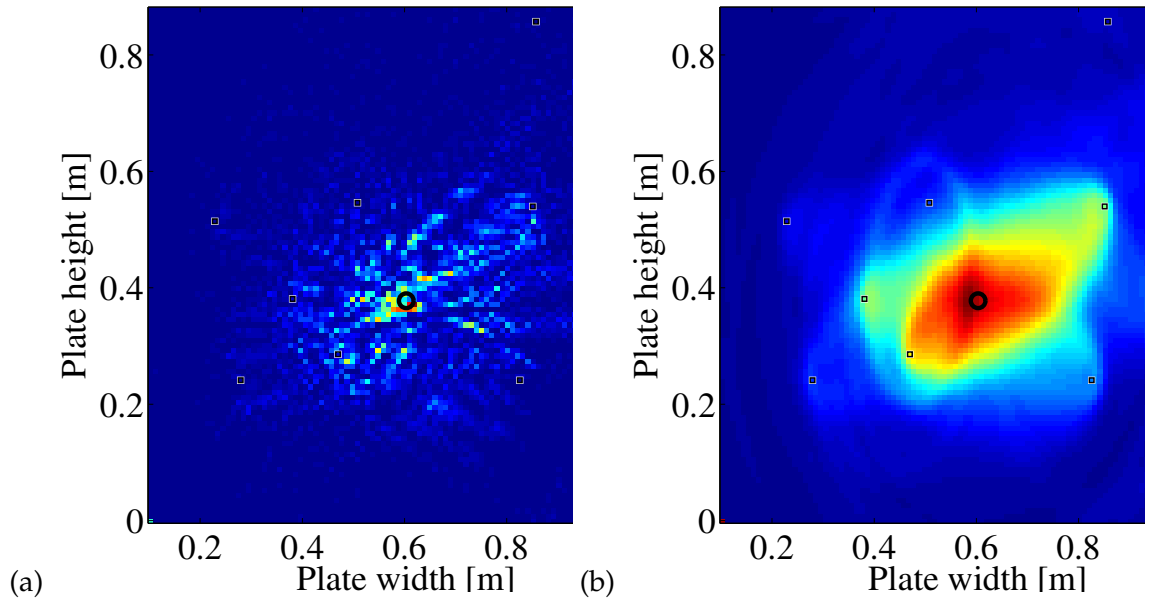

Figure 3.5. Illustrates damage detection in unidirectional composite plate. (a) coherent matched field processor, (b) the sensor domain incoherent matched field processor.

3.5 Conclusion

This chapter showed the implementation of the coherent and the sensor domain incoherent data-driven matched field processor to localize a scatterer on a carbon-fiber and glass-fiber composite plate using experimental data. The sparsity-based data-driven model is created using sparse wavenumber analysis and sparse wavenumber synthesis as discussed in Chapter 2. This data-driven model is then integrated with matched field processing for localization.

Our data-driven approach localizes the scatterer successfully whereas the delay-and-sum methods could not localize it. The data-driven matched field processing approach combines the information about the medium directly from data and hence provides more accurate localization than the delay-and-sum approach.

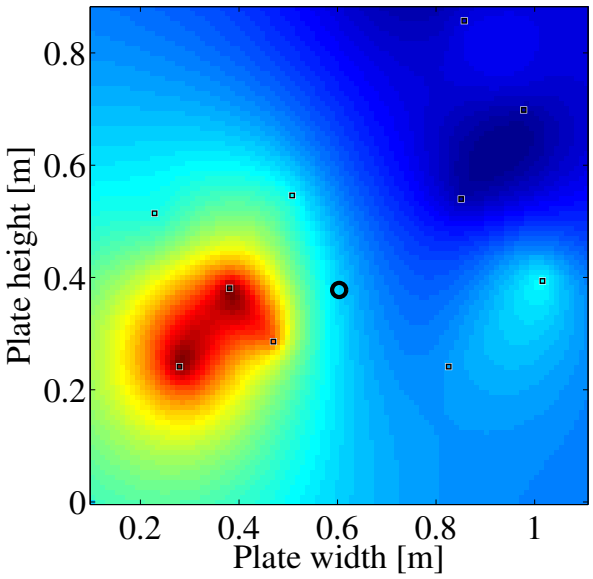

Figure 3.6. Illustrates damage detection in unidirectional composite plate using delay-and-sum. The bold circle represents the scatterer.

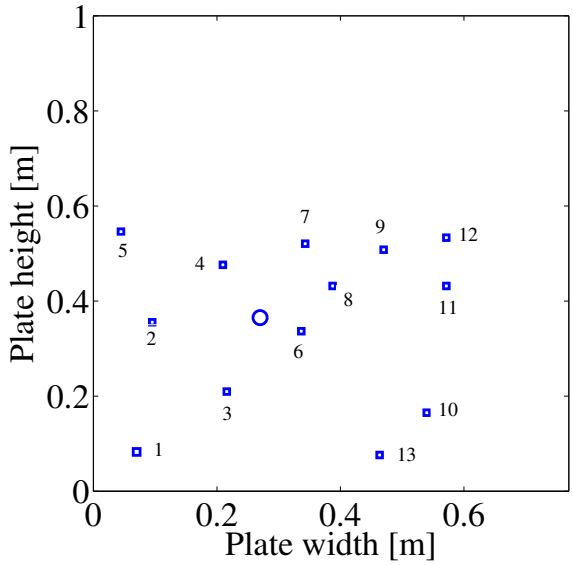

Figure 3.7. Illustration of glass fiber composite plate used for our experimental setup. Each square represents a transducer and bold circle represents the scatterer (mass).

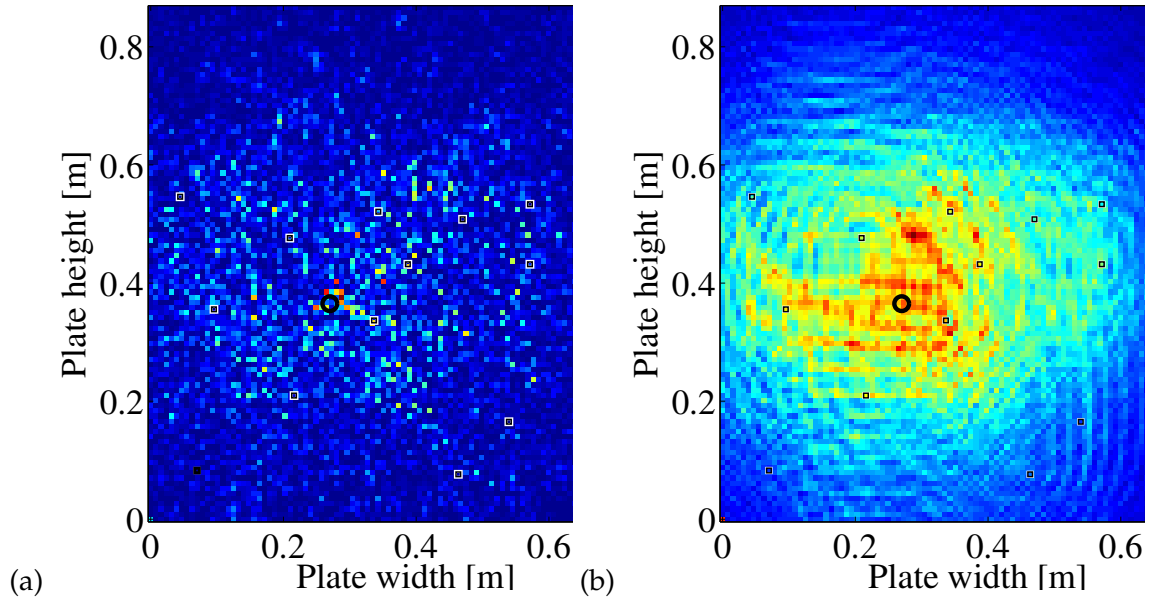

Figure 3.8. Illustrates damage detection in glass-fiber composite plate. (a) coherent matched field processor, (b) the sensor domain incoherent matched field processor.

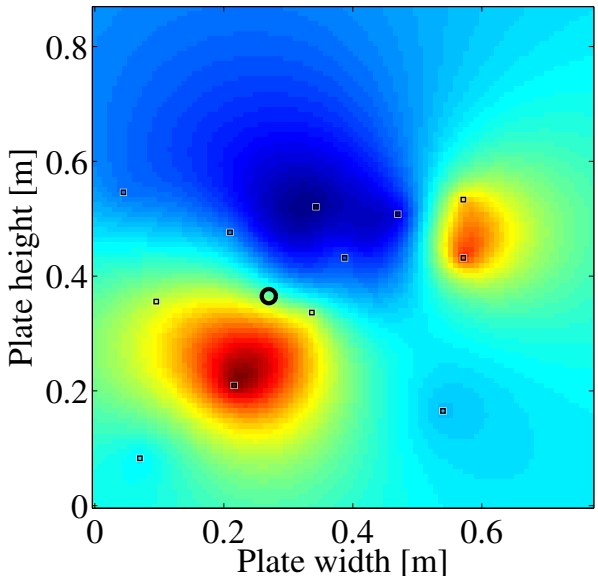

Figure 3.9. Illustrates damage detection in glass-fiber composite plate using delay-and–sum. The bold circle represents the scatterer.

CHAPTER 4

CONCLUSION AND FUTURE WORK

4.1 Summary

In this thesis, we created an approximate model for anisotropy by characterizing the wave propagation in horizontal and vertical directions. Using orthogonal matching pursuit, a compressive sensing algorithm, we recovered the frequency-wavenumber representation, or dispersion curves, of guided waves in a composite structure. This process is called sparse wavenumber analysis.

Using this frequency-wavenumber representation, we generated a data-driven model of guided wave propagation in an anisotropic medium. This is called sparse wavenumber synthesis. This data-driven model is integrated with a matched field processor to locate a damage on a composite structure. The results from our method are more accurate in damage localization than the traditional delay-and-sum approach.

The methodologies created in this thesis are

1. **Sparse wavenumber analysis**

   We accurately recovered the frequency-wavenumber characteristics, or dispersion curves, of the guided waves using a compressive sensing algorithm (Chapter 2).

2. **Sparse wavenumber synthesis**

   We generated a sparsity-based data-driven model, which predicts the Lamb wave response between any two points in the medium (Chapter 2).

3. **Coherent data-driven matched field processor**

   We successfully localized a scatterer on a carbon-fiber and glass-fiber composite plate (Chapter 3).

4. **Sensor domain incoherent data-driven matched field processor**

Sensor domain incoherent data matched field processor provides better resolution for damage localization than a coherent matched field processor (Chapter 3).

These techniques can detect and locate damage in a carbon-fiber and glass-fiber composite plate. In the following section, we will discuss the future scope of this work.

4.2 Future Work

For our future work, we plan to improve our data-driven model for more accurate damage localization. Our localization is not perfect. We can observe from Figure 3.8 that localization has noisy results. One source of error might be reflections from the boundaries of the plate that are not part of our model in (2.2). Hence, incorporating the removal of reflections from the data will help in improving the performance of sparse wavenumber analysis and sparse wavenumber synthesis.

The model can be further tested on different composite plates such as quasi-isotropic and orthotropic composite plates. A quasi-isotropic composite has isotropic properties in-plane. Generally, a quasi-isotropic composite has plies oriented at 0°, 90°, $+45^\circ$, and -45°. An orthotropic plate has different properties in three mutually perpendicular directions having two fold rotational symmetry about an axis.

We can also refine our data-driven matched field processor to localize multiple damages on the plate.

REFERENCES

[1] H. Sohn, C. R. Farrar, F. M. Hemez, D. D. Shunk, D. W. Stinemates, B. R. Nadler, and J. J. Czarnecki, "A review of structural health monitoring literature: 1996–2001," Los Alamos National Laboratory, USA, Tech. Rep., 2003.

[2] W. Staszewski, C. Boller, and G. R. Tomlinson, *Health Monitoring of Aerospace Structures: Smart Sensor Technologies and Signal Processing*. John Wiley & Sons, 2004.

[3] V. Giurgiutiu, *Structural Health Monitoring with Piezoelectric Wafer Active Sensors*. Academic Press, 2007.

[4] D. Balageas, C.-P. Fritzen, and A. Güemes, *Structural Health Monitoring*. John Wiley & Sons, 2010, vol. 90.

[5] A. Gorlov, "Disaster of the i-95 mianus river bridge. where could lateral vibration come from?" *Journal of Applied Mechanics*, vol. 51, no. 3, pp. 694–696, 1984.

[6] Z. Kral, W. J. Horn, and J. E. Steck, "Damage detection in metal structures using acoustic emission," *In Proceedings: 5th Annual Symposium: Graduate Research and Scholarly Projects*, 2009.

[7] K. Diamanti and C. Soutis, "Structural health monitoring techniques for aircraft composite structures," *Progress in Aerospace Sciences*, vol. 46, no. 8, pp. 342–352, 2010.

[8] M. D. Seale and E. I. Madaras, "Lamb wave characterization of the effects of long-term thermal-mechanical aging on composite stiffness," *The Journal of the Acoustical Society of America*, vol. 106, no. 3, pp. 1346–1352, 1999.

[9] R. Talreja, "Fatigue of composite materials: damage mechanisms and fatigue-life diagrams," in *Proceedings of the Royal Society of London A: Mathematical, Physical and Engineering Sciences*, vol. 378, no. 1775. The Royal Society, 1981, pp. 461–475.

[10] C. Ng and M. Veidt, "Scattering analysis of fundamental anti-symmetric lamb wave at delaminations in composite laminates," *Australian Journal of Mechanical Engineering*, vol. 8, no. 2, pp. 197–205, 2011.

[11] T. Monnier, "Lamb waves-based impact damage monitoring of a stiffened aircraft panel using piezoelectric transducers," *Journal of Intelligent Material Systems and Structures*, vol. 17, no. 5, pp. 411–421, 2006.

[12] S. K. Chakrapani, D. Barnard, V. Dayal, D. E. Chimenti, L. J. Bond, and D. O. Thompson, "Detection of in-plane fiber waviness in composite laminates using guided lamb modes," in *AIP Conference Proceedings*, vol. 1581, no. 1. AIP, 2014, pp. 1134–1140.

[13] H. Sohn, G. Park, J. R. Wait, N. P. Limback, and C. R. Farrar, "Wavelet-based active sensing for delamination detection in composite structures," *Smart Materials and Structures*, vol. 13, no. 1, p. 153, 2003.

[14] K. Balasubramaniam and J. L. Rose, "Physically based dispersion curve feature analysis in the nde of composites," *Journal of Research in Nondestructive Evaluation*, vol. 3, no. 1, pp. 41–67, 1991.

[15] J. Blitz and G. Simpson, *Ultrasonic methods of non-destructive testing*. Springer Science & Business Media, 1995, vol. 2.

[16] Z. Su, L. Ye, and Y. Lu, "Guided lamb waves for identification of damage in composite structures: A review," *Journal of Sound and Vibration*, vol. 295, no. 3, pp. 753–780, 2006.

[17] J. B. Harley and J. M. Moura, "Sparse recovery of the multimodal and dispersive characteristics of lamb waves," *The Journal of the Acoustical Society of America*, vol. 133, no. 5, pp. 2732–2745, 2013.

[18] J. E. Michaels, "Detection, localization and characterization of damage in plates with an in situ array of spatially distributed ultrasonic sensors," *Smart Materials and Structures*, vol. 17, no. 3, p. 035035, 2008.

[19] T. Kundu, H. Nakatani, and N. Takeda, "Acoustic source localization in anisotropic plates," *Ultrasonics*, vol. 52, no. 6, pp. 740–746, 2012.

[20] J. B. Harley and J. M. Moura, "Data-driven matched field processing for lamb wave structural health monitoring," *The Journal of the Acoustical Society of America*, vol. 135, no. 3, pp. 1231–1244, 2014.

[21] L. Van Den Einde, L. Zhao, and F. Seible, "Use of frp composites in civil structural applications," *Construction and Building Materials*, vol. 17, no. 6, pp. 389–403, 2003.

[22] Y. Zou, L. Tong, and G. P. Steven, "Vibration-based model-dependent damage (delamination) identification and health monitoring for composite structuresa review," *Journal of Sound and vibration*, vol. 230, no. 2, pp. 357–378, 2000.

[23] H. Hsiao and I. Daniel, "Effect of fiber waviness on stiffness and strength reduction of unidirectional composites under compressive loading," *Composites Science and Technology*, vol. 56, no. 5, pp. 581–593, 1996.

[24] C. A. Steeves and N. A. Fleck, "In-plane properties of composite laminates with through-thickness pin reinforcement," *International Journal of Solids and Structures*, vol. 43, no. 10, pp. 3197–3212, 2006.

[25] R. Smith, "Composite defects and their detection," *Materials Science and Engineering*, vol. 3, pp. 103–143, 2009.

[26] D. K. Hsu and H. Jeong, "Ultrasonic velocity change and dispersion due to porosity in composite laminates," in *Review of Progress in Quantitative Nondestructive Evaluation*. Springer, 1989, pp. 1567–1573.

[27] L. Knopoff and J. Schlue, "Rayleigh wave phase velocities for the path addis ababa-nairobi," *Tectonophysics*, vol. 15, no. 1-2, pp. 157 161–158 163, 1972.

[28] Z.-X. Zhang, *Rock Fracture and Blasting: Theory and Applications*. Butterworth-Heinemann, 2016.

[29] J. Achenbach, *Wave propagation in elastic solids*. Elsevier, 2012, vol. 16.

[30] B. Jakoby and M. J. Vellekoop, "Properties of love waves: applications in sensors," *Smart Materials and Structures*, vol. 6, no. 6, p. 668, 1997.

[31] M. N. Ahmed, "A study of guided ultrasonic wave propagation characteristics in thin aluminum plate for damage detection," Ph.D. dissertation, University of Toledo, 2014.

[32] P. Fromme, P. D. Wilcox, M. J. Lowe, and P. Cawley, "On the development and testing of a guided ultrasonic wave array for structural integrity monitoring," *IEEE Transactions on Ultrasonics, Ferroelectrics, and Frequency Control*, vol. 53, no. 4, pp. 777–785, 2006.

[33] J. E. Michaels and T. E. Michaels, "An integrated strategy for detection and imaging of damage using a spatially distributed array of piezoelectric sensors," in *Proc. SPIE Conf. on Health Monitoring of Structural and Biological Systems; Proc. SPIE*, vol. 6532, 2007, p. 653203.

[34] J. E. Michaels, A. J. Croxford, and P. D. Wilcox, "Imaging algorithms for locating damage via in situ ultrasonic sensors," in *Sensors Applications Symposium*. IEEE, 2008, pp. 63–67.

[35] J. B. Harley, N. Thavornpitak, J. M. Moura, D. O. Thompson, and D. E. Chimenti, "Delay-and-sum technique for localization of active sources in cylindrical objects," in *AIP Conference Proceedings*, vol. 1511, no. 1. AIP, 2013, pp. 294–301.

[36] G. Lu, Y. Li, T. Wang, H. Xiao, L. Huo, and G. Song, "A multi-delay-and-sum imaging algorithm for damage detection using piezoceramic transducers," *Journal of Intelligent Material Systems and Structures*, p. 1045389X16666184, 2016.

[37] C. H. Wang, J. T. Rose, and F.-K. Chang, "A synthetic time-reversal imaging method for structural health monitoring," *Smart Materials and Structures*, vol. 13, no. 2, p. 415, 2004.

[38] Z. Sharif-Khodaei and M. Aliabadi, "Assessment of delay-and-sum algorithms for damage detection in aluminium and composite plates," *Smart Materials and Structures*, vol. 23, no. 7, p. 075007, 2014.

[39] L. Qiu, M. Liu, X. Qing, and S. Yuan, "A quantitative multidamage monitoring method for large-scale complex composite," *Structural Health Monitoring*, vol. 12, no. 3, pp. 183–196, 2013.

[40] H. Sohn, H. W. Park, K. H. Law, and C. R. Farrar, "Damage detection in composite plates by using an enhanced time reversal method," *Journal of Aerospace Engineering*, vol. 20, no. 3, pp. 141–151, 2007.

[41] R. Watkins and R. Jha, "A modified time reversal method for lamb wave based diagnostics of composite structures," *Mechanical Systems and Signal Processing*, vol. 31, pp. 345–354, 2012.

[42] E. J. Candès and M. B. Wakin, "An introduction to compressive sampling," *IEEE Signal Processing Magazine*, vol. 25, no. 2, pp. 21–30, 2008.

[43] D. L. Donoho, "Compressed sensing," *IEEE Transactions on information theory*, vol. 52, no. 4, pp. 1289–1306, 2006.

[44] Y. C. Eldar and G. Kutyniok, *Compressed sensing: theory and applications*. Cambridge University Press, 2012.

[45] E. Candes and T. Tao, "Computer-implemented method for correcting transmission errors using linear programming," Apr. 2 2013, uS Patent 8,413,019.

[46] E. J. Candes, "The restricted isometry property and its implications for compressed sensing," *Comptes Rendus Mathematique*, vol. 346, no. 9-10, pp. 589–592, 2008.

[47] M. Eybpoosh, M. Berges, and H. Y. Noh, "Sparse representation of ultrasonic guided-waves for robust damage detection in pipelines under varying environmental and operational conditions," *Structural Control and Health Monitoring*, vol. 23, no. 2, pp. 369–391, 2016.

[48] S. S. Chen, D. L. Donoho, and M. A. Saunders, "Atomic decomposition by basis pursuit," *SIAM Review*, vol. 43, no. 1, pp. 129–159, 2001.

[49] J. B. Harley and J. M. Moura, "Dispersion curve recovery with orthogonal matching pursuit," *The Journal of the Acoustical Society of America*, vol. 137, no. 1, pp. EL1–EL7, 2015.

[50] J. B. Harley and J. M. Mourn, "Matched field processing localization with random sensor topologies," in *Acoustics, Speech and Signal Processing (ICASSP)*. IEEE, 2014, pp. 1404–1408.

[51] D. B. Harris and T. Kvaerna, "Superresolution with seismic arrays using empirical matched field processing," *Geophysical Journal International*, vol. 182, no. 3, pp. 1455–1477, 2010.

[52] C. Debever and W. Kuperman, "Robust matched-field processing using a coherent broadband white noise constraint processor," *The Journal of the Acoustical Society of America*, vol. 122, no. 4, pp. 1979–1986, 2007.

[53] D. Alleyne and P. Cawley, "A two-dimensional fourier transform method for the measurement of propagating multimode signals," *The Journal of the Acoustical Society of America*, vol. 89, no. 3, pp. 1159–1168, 1991.

[54] Y. Wang, Z. Longxiang, L. Fan, and S. Fengrui, "Guided waves modes identification in pipes detection by application of the matching pursuit method," in *Electronic Measurement & Instruments (ICEMI), 2011 10th International Conference on*, vol. 4. IEEE, 2011, pp. 50–53.

[55] W. Prosser, M. D. Seale, and B. T. Smith, "Time-frequency analysis of the dispersion of lamb modes," *The Journal of the Acoustical Society of America*, vol. 105, no. 5, pp. 2669–2676, 1999.

[56] M. Niethammer, L. J. Jacobs, J. Qu, and J. Jarzynski, "Time-frequency representation of lamb waves using the reassigned spectrogram," *The Journal of the Acoustical Society of America*, vol. 107, no. 5, pp. L19–L24, 2000.

[57] C. Lane, *Wave Propagation in Anisotropic Media*. Cham: Springer International Publishing, 2014, pp. 13–39.

[58] J. B. Harley, "Predictive guided wave models through sparse modal representations," *Proceedings of the IEEE*, vol. 104, no. 8, 2016.

[59] S. E. Dosso and M. J. Wilmut, "Maximum-likelihood and other processors for incoherent and coherent matched-field localization," *The Journal of the Acoustical Society of America*, vol. 132, no. 4, pp. 2273–2285, 2012.